PHILOSOPHICAL TRANSACTIONS A

rsta.royalsocietypublishing.org

Research

Cite this article: Tekoğlu C, Hutchinson JW, Pardoen T. 2015 On localization and void coalescence as a precursor to ductile fracture. *Phil. Trans. R. Soc. A* **373**: 20140121. http://dx.doi.org/10.1098/rsta.2014.0121

One contribution of 19 to a theme issue 'Fracturing across the multi-scales of diverse materials'.

Subject Areas:
materials science

Keywords:
ductile fracture, localization, void coalescence, Lode parameter, shear

Author for correspondence:
C. Tekoğlu
e-mail: c.tekoglu@gmail.com

Electronic supplementary material is available at http://dx.doi.org/10.1098/rsta.2014.0121 or via http://rsta.royalsocietypublishing.org.

THE ROYAL SOCIETY PUBLISHING

On localization and void coalescence as a precursor to ductile fracture

C. Tekoğlu[1], J. W. Hutchinson[2] and T. Pardoen[3]

[1]Department of Mechanical Engineering, TOBB University of Economics and Technology, Söğütözü, Ankara 06560, Turkey
[2]School of Engineering and Applied Sciences, Harvard University, Cambridge, MA 02138, USA
[3]Institute of Mechanics, Materials and Civil Engineering, Université catholique de Louvain, Place Sainte Barbe, 2, B-1348 Louvain-la-Neuve, Belgium

Two modes of plastic flow localization commonly occur in the ductile fracture of structural metals undergoing damage and failure by the mechanism involving void nucleation, growth and coalescence. The first mode consists of a macroscopic localization, usually linked to the softening effect of void nucleation and growth, in either a normal band or a shear band where the thickness of the band is comparable to void spacing. The second mode is coalescence with plastic strain localizing to the ligaments between voids by an internal necking process. The ductility of a material is tied to the strain at macroscopic localization, as this marks the limit of uniform straining at the macroscopic scale. The question addressed is whether macroscopic localization occurs prior to void coalescence or whether the two occur simultaneously. The relation between these two modes of localization is studied quantitatively in this paper using a three-dimensional elastic–plastic computational model representing a doubly periodic array of voids within a band confined between two semi-infinite outer blocks of the same material but without voids. At sufficiently high stress triaxiality, a clear separation exists between the two modes of localization. At lower stress triaxialities, the model predicts that the onset of macroscopic localization and coalescence occur simultaneously.

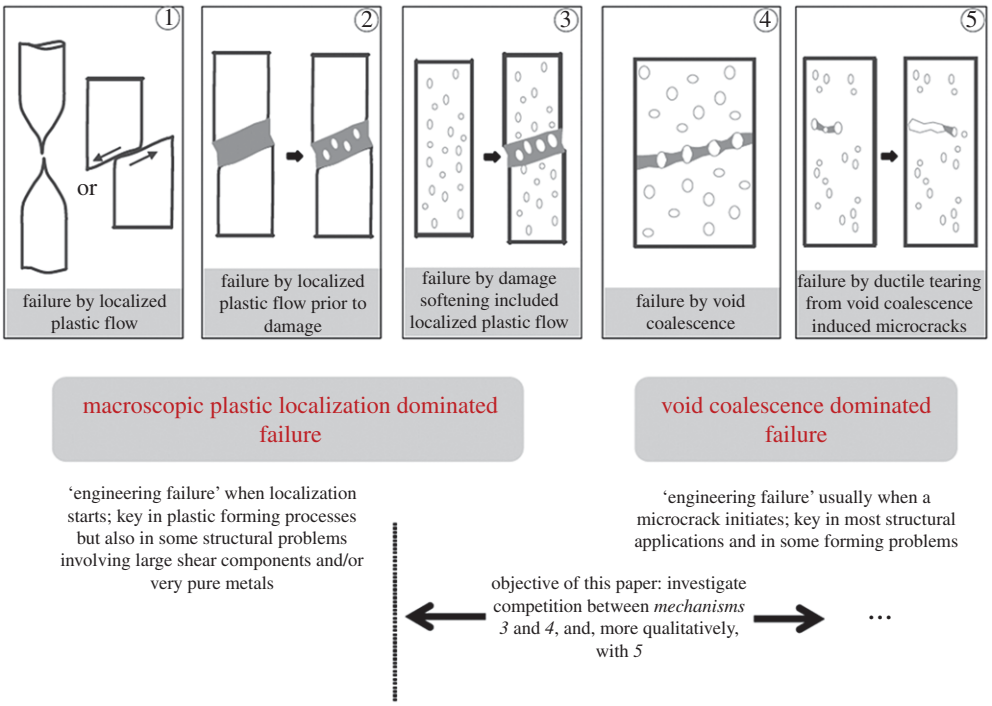

Figure 1. The five generic scenarios of ductile fracture in single phase polycrystals at temperatures far below melting temperature. The objective of the paper is to investigate the competition between *mechanisms 3* and *4*, with implications for *mechanism 5*. (Online version in colour.)

1. Introduction

Ductile fracture is the main failure mechanism impacting forming process analysis and is central in structural integrity assessment together with fatigue and corrosion. One of the obvious reasons is that the properties of structural metallic alloys are continually improved to avoid cleavage and other types of intergranular fracture leaving void nucleation, growth and coalescence as the dominant damage mechanism. Beginning with the early observational [1] and mechanics [2,3] work on the role of void growth in ductile fracture, the micromechanics-based approach of ductile fracture has been developed to overcome some of the limitations of fracture mechanics when dealing with ductile, tough structural alloys providing a direct link with the material microstructure and physics [4–11]. This link is essential for guiding materials scientists in the development of better alloys. Furthermore, a micromechanics-based approach can also be used to address plastic-forming processes, e.g. [12–14]. Although the field of ductile fracture has received attention for more than 50 years, continually striving for more reliable damage models and localization criteria, the field is rich with new challenges. These include capitalizing on recent experimental and theoretical developments related to stress state dependence [15–18], development of computational models capable of predicting both crack initiation and crack advance [7–11,19–22], applications to extensive tearing of plates and sheets [23–26], further progress in void growth and coalescence models [27–32] and the challenge of localization and fracture under distinctly non-proportional straining and stressing histories such as those often encountered in forming processes.

Figure 1 provides a schematic of some of the many possible failure scenarios, or mechanisms, that are usually covered by the term 'ductile fracture'. Figure 1 also serves to position the scope of this work within the larger scheme. The focus of this paper is on the micromechanics of the

last two stages of void nucleation, growth and coalescence. Nucleation of voids or microcracks by cracking and debonding of second phase particles is often an essential step in the failure process. Increasing nucleation resistance is an important means for improving ductility, and advances in the micromechanics of nucleation are also essential to improving alloy ductility. High temperature ductile fracture, where creep and viscoplasticity can play an important role as well as complexities associated with composite or multiphase alloys have not been addressed in figure 1. Similarly, adiabatic localization under high strain rate deformation is not covered in figure 1 and in our analysis.

Mechanism 1 takes place for very pure metals only. Clean single crystal or polycrystalline metals sometimes fail without any occurrence of damage owing to the absence of void nucleation sites. After a stage of homogeneous plastic deformation, plastic flow localizes inside a diffuse neck or in a shear band, and the flow continues until material separation. High pressure superimposed on a material can suppress other mechanisms as well allowing this mechanism to prevail.

Mechanism 2 corresponds to the localization of plasticity into shear bands within a non-porous material owing to various possible softening mechanisms, often arising at the scale of the single crystal grains. Subsequently, following the accumulation of large plastic strains inside the band, voids nucleate, grow and coalesce to produce final material separation. This mechanism can occur at the tip of a crack. Recent work by Morgeneyer *et al*. [33], using a three-dimensional *in situ* laminography technique, clearly reveals that plastic localization in front of a crack in an Al alloy occurs prior to void nucleation.

Mechanism 3 involves damage nucleation in the material prior to macroscopic localization. The softening induced by the accumulated porosity is sufficient to counteract the strain-hardening capacity of the material and leads to plastic localization in a narrow band. A general framework for analysing macroscopic localization in elastic–plastic solids represented by continuum constitutive models was presented by Rice [34]. Mechanism-based continuum models which incorporate the softening effects of void nucleation and growth appeared at roughly the same time [35]. Fracture surfaces of materials failing under *mechanisms 2* or *3* exhibit dimples representing the final state of the voids that have greatly enlarged during the growth and coalescence taking place after the onset of macroscopic localization when all the straining occurs in the band. The connection between the voids in the initial and final states is often not easily readily apparent owing to large shear distortions.

Mechanism 4 has macroscopic localization and coalescence occurring simultaneously without requiring prior localization owing to the growth mechanism. In this case, the onset of coalescence dictates the onset of macroscopic localization. One of the primary aims of the present paper is to clarify the distinction between *mechanisms 3* and *4* and to ascertain when they occur separately or simultaneously. Void coalescence has received a considerable attention in recent years with significant refinements of the early models of Thomason [36], as illustrated in references [28,31]. Void coalescence has also been incorporated in an ad hoc manner in the continuum models for porous elastic–plastic solids [5].

Mechanism 5 could be regarded as a subset of *mechanism 4*, but it is identified separately in figure 1 to distinguish between coalescence localizations extending over many voids and those involving just a few voids—one might say to distinguish between macroscopic and cluster localizations. This paper focuses on macroscopic localizations whether owing to void growth or coalescence. Nevertheless, experiments relying on *in situ* three-dimensional microtomography [37,38] provide ample evidence that cluster localizations commonly occur. Furthermore, crack advance in ductile structural metals suggests that the two mechanisms are distinct [39]. Crack growth can occur by the void-by-void mechanism modelled by Rice & Johnson [40], wherein the crack tip coalesces with the closest void, or it may occur in a manner in which an extended macroscopic normal localization zone forms ahead of the tip, as modelled by Tvergaard & Hutchinson [41]. In a structural alloy subjected to non-uniform deformation, cluster coalescence will often take place in a region involving a few more closely spaced voids and/or experiencing larger local stress triaxiality or plastic strain. Coalescence of these few voids can lead to a microcrack which then propagates through repeated coalescence between the crack tip and the

neighbouring voids. The rest of the failure process is thus a ductile tearing process. Compared with modelling efforts to understand *mechanism 3* and *4*, relatively little effort has gone into modelling cluster localization and fully account for effects of heterogeneities [42].

The onset of macroscopic localization serves as an effective indicator of a material's ductility for engineering purposes because it is the precursor to failure and it marks the limit of the uniform strain that can be imposed on the material. Nevertheless, there appears to be considerable confusion in the literature between the two types of plastic localizations: macroscopic localization driven by damage softening (*mechanism 3*) where plastic flow engulfs the voids in the band whose width is set largely by void spacing, and void coalescence (*mechanism 4*) where the band width is more narrow with continuing plastic deformation limited to the ligaments between neighbouring voids. The distinction between these two modes of localization was evident in the pioneering computational work on void growth and localization of Koplik & Needleman [43] and Tvergaard [44]. Perhaps the more recent confusion surrounding the two modes stems from the fact that coalescence may occur as a secondary localization within an earlier localization and that the earlier work did not attempt to quantify the distinction between them. As noted above, this is one of the primary objectives of this paper. In addition, in the discussion of the results, we raise the issue of whether the class of models used here, and in almost all computational studies to date which employ aligned periodic arrays of voids, might be too idealized to realistically capture when macroscopic localization precedes coalescence.

The model, along with details related to its numerical implementation issues, is presented in §2 with some details given in the electronic supplementary material. Results of the simulations are presented and discussed in depth in §3. Section 4 contains the final summary, discussion of open questions and suggestions for further research.

2. Numerical methods

A three-dimensional finite-element (FE) framework is developed to investigate the localization of plastic flow in an infinite block containing a porous band. The FE model is similar in some respects to the models introduced by Tvergaard [45], Barsoum & Faleslog [15] and Dunand & Mohr [16]. The model is assumed to be composed of three regions: two semi-infinite blocks of uniform material but void-free, separated by an infinite planar band containing a doubly periodic array of initially spherical voids, as depicted in figure 2. Apart from the existence of the voids in the band, the material is uniform through the three regions. This class of models generates a detailed three-dimensional FE analysis of growth and interaction of the voids within the band. Macroscopic localization is identified as the point in the overall straining history when a limit is reached such that elastic unloading occurs within the two outer blocks and plastic straining continues in the band. This definition of macroscopic localization is consistent with that introduced in Rice's [34] general localization analysis carried out within the framework of continuum constitutive behaviour and with the earlier two-dimensional model of sheet metal necking of Marciniak & Kuczynski [46]. The explicit three-dimensional analysis of the void growth and interaction in the band eliminates the need to invoke a continuum constitutive model of a porous elastic–plastic material. Thus, the present class of models has much in common with periodic cell models employed in many earlier studies [43–45,47,48]. However, by incorporating the outer blocks into the present model, it is possible to more realistically capture the behaviour in the localization band after the onset of macroscopic localization. By continuing the analysis in the band beyond the onset of macroscopic localization, one is able to study and compute the onset of void coalescence, as will be done in this paper.

Figure 2 shows both the global coordinate system with axes x_i and the local coordinate system attached to the band (and therefore rotating with the band) with axes ξ_i ($i = 1, 2, 3$). The band contains a square array of voids periodically distributed in the ξ_1- and ξ_3-directions. The top and bottom surfaces of the band are parallel to the ξ_1-axis, and the ξ_3- and x_3-axes are parallel to each other. The orientation angle of the band in the undeformed (initial) state is noted ψ^{u}. The semi-infinite outer blocks are subjected to overall uniform straining parallel to the principal stress axes

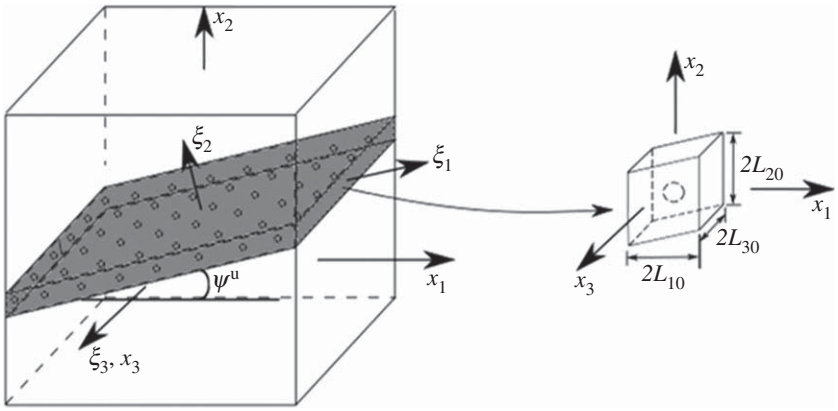

Figure 2. The model is assumed to be composed of three regions: two semi-infinite blocks of uniform material but void-free separated by an infinite planar porous band, the dark grey region. The band contains an array of initially spherical voids that is doubly periodic in the ξ_1- and ξ_3-directions. Owing to the periodic distribution of the voids, the band can be modelled as a parallelepiped unit cell containing a void in its centre, as shown in the figure. The orientation angle of the band in the undeformed (initial) state, ψ^u, is a variable in the problem and all possible orientations have to be considered. Note that $L_{10} = L_0 \times \cos(\psi^u)$, $L_{20} = L_0/\cos(\psi^u)$, and $L_{30} = L_0$, and the initial volume of the unit cell is $V^{cell} = 8L_0^3$ for any angle ψ^u.

which are in turn fixed with respect to the x_i axes, leading to a triaxial stress state with $\Sigma_{22} \equiv \Sigma_I > \Sigma_{33} \equiv \Sigma_{II} > \Sigma_{11} \equiv \Sigma_{III}$, where Σ_{ij} is the Cauchy stress tensor and $\Sigma_I, \Sigma_{II}, \Sigma_{III}$ are the principal stresses components. For the loading considered, the normal to the plane of the localization band can be anticipated to always be perpendicular to the ξ_3- and x_3-axes. The orientation angle of the band at any stage of deformation, ψ, evolves with the deformation of the outer blocks as

$$\left.\begin{aligned} \tan(\psi) &= e^{(E_{22}-E_{11})}\tan(\psi^u) \\ \text{and} \qquad \dot{\psi} &= \tfrac{1}{2}\sin(2\psi)(\dot{E}_{22} - \dot{E}_{11}), \end{aligned}\right\} \tag{2.1}$$

where E_{11}, E_{22} and E_{33} are the logarithmic strains in the outer blocks defined in terms of the stretches as

$$E_{11} = \ln(\lambda_1), \quad E_{22} = \ln(\lambda_2), \quad E_{33} = \ln(\lambda_3). \tag{2.2}$$

The stress triaxiality T, Lode parameter L and effective stress Σ_{eq} describing the stress state in the outer blocks are

$$T = \frac{\Sigma_I + \Sigma_{II} + \Sigma_{III}}{3\Sigma_{eq}}, \tag{2.3}$$

$$L = \frac{2\Sigma_{II} - \Sigma_I - \Sigma_{III}}{\Sigma_I - \Sigma_{III}} \tag{2.4}$$

and

$$\Sigma_{eq} = \sqrt{\frac{1}{2}[(\Sigma_I - \Sigma_{II})^2 + (\Sigma_I - \Sigma_{III})^2 + (\Sigma_{II} - \Sigma_{III})^2]}. \tag{2.5}$$

Calculations are performed under constant prescribed T and L values in the outer blocks over the relevant range of initial band orientations with true stress increments satisfying

$$\left.\begin{aligned} &\dot{\Sigma}_{22} = \dot{\Sigma}_I, \quad \dot{\Sigma}_{11} = Q\dot{\Sigma}_I, \quad \dot{\Sigma}_{33} = R\dot{\Sigma}_I, \\ &\dot{\Sigma}_{eq} = \dot{\Sigma}_I\sqrt{\frac{1}{2}[(1-R)^2 + (1-Q)^2 + (R-Q)^2]}. \end{aligned}\right\} \tag{2.6}$$

The constant coefficients satisfy $Q \le R \le 1$ and can be directly expressed in terms of T and L.

The material in the outer blocks, as well as that in the band containing the voids, is modelled by finite strain J_2 flow theory with isotropic elasticity. The inputs characterizing the material are Young's modulus, E, Poisson's ratio, ν, and the relation of the true stress to the effective logarithmic plastic strain in uniaxial tension, $\sigma_{\mathrm{M}}(E^{\mathrm{P}}_{\mathrm{eq}})$. In Cartesian coordinates, the relation between the Eulerian strain rate, D_{ij}, and the Jaumann stress rate, $\hat{\Sigma}_{ij}$, is $D_{ij} = M_{ijkl}\hat{\Sigma}_{kl}$ with

$$M_{ijkl} = \frac{1+\nu}{2E}(\delta_{ik}\delta_{jl} + \delta_{il}\delta_{jk}) - \frac{\nu}{E}\delta_{ij}\delta_{kl} + \frac{9S_{ij}S_{ij}}{h\,\sigma_{\mathrm{M}}(E^{\mathrm{P}}_{\mathrm{eq}})^2}, \tag{2.7}$$

where S_{ij} is the stress deviator and $h = \mathrm{d}\sigma_{\mathrm{M}}(E^{\mathrm{P}}_{\mathrm{eq}})/\mathrm{d}E^{\mathrm{P}}_{\mathrm{eq}}$. With D^{P}_{ij} denoting the plastic part of the Eulerian strain rate and $\dot{E}^{\mathrm{P}}_{\mathrm{eq}} = \sqrt{3D^{\mathrm{P}}_{ij}D^{\mathrm{P}}_{ij}/2}$, $E^{\mathrm{P}}_{\mathrm{eq}} = \int \dot{E}^{\mathrm{P}}_{\mathrm{eq}}$ is the accumulated equivalent logarithmic plastic strain. Equation (2.7) applies for plastic loading; for elastic loading, the last term in (2.7) is deleted. The inverse of (2.7) is denoted by $\hat{\Sigma}_{ij} = L_{ijkl}D_{kl}$.

In the outer blocks in the x_i-coordinates, $\dot{E}_{11} = D_{11}, \dot{E}_{22} = D_{22}$ and $\dot{E}_{33} = D_{33}$, and the true stress rates coincide with the Janmann rates such that $\dot{\Sigma}_{\mathrm{I}} = \hat{\Sigma}_{22}$, etc. The incremental strain–stress relationship can be expressed in terms of the applied maximum principal stress rate, $\dot{\Sigma}_{\mathrm{I}}$, and the specified T- and L-values using (2.7). The corresponding displacement field in the upper block outside the band reads

$$u_1 = (\lambda_1 - 1)x_1 + \Delta_1, \quad u_2 = (\lambda_2 - 1)x_2 + \Delta_2, \quad u_3 = (\lambda_3 - 1)x_3, \tag{2.8}$$

and in the lower block outside the band

$$u_1 = (\lambda_1 - 1)x_1 - \Delta_1, \quad u_2 = (\lambda_2 - 1)x_2 - \Delta_2, \quad u_3 = (\lambda_3 - 1)x_3. \tag{2.9}$$

The additional rigid body displacements of the outer blocks relative to one another ($2\Delta_1$ and $2\Delta_2$) reflect the fact that band is weaker than the outer blocks and undergoes different strains. By symmetry, there is no relative displacement of the outer blocks in the x_3-direction. The additional displacements Δ_1 and Δ_2 would vanish if the band contained no voids.

In setting the boundary conditions for one of the periodic unit cells within the band, it is assumed that the initially planar interfaces between the band and the outer blocks remain planar and parallel as deformation proceeds. In reality, the planar periodic array of voids within the band slightly perturbs the cell/block interface with the same periodicity. This effect, however, is considered to be very small and neglected in the present model. The displacement rates at the top and bottom faces of the band read

$$\dot{U}_1 = \dot{\lambda}_1 x_1 \pm \dot{\Delta}_1, \quad \dot{U}_2 = \dot{\lambda}_2 x_2 \pm \dot{\Delta}_2, \quad \dot{U}_3 = \dot{\lambda}_3 x_3. \tag{2.10}$$

Owing to the symmetries of the problem, the faces of the unit cell with a normal in the x_3-direction remain planar, and the boundary conditions on these faces correspond to a normal displacement increment given by the third equation in (2.10) and zero shear tractions. The faces with a normal in the x_1-direction in the undeformed cell (denoted as 'surface-left' and 'surface-right' in figure 3) distort as deformation proceeds: they become non-planar, but with the normal at any point lying in the (x_1, x_2) plane. These faces must satisfy periodicity conditions on displacement and traction increments with the left and right faces displacing relative to one another in a manner consistent with the displacements at the top and bottom edges of the faces. Equations involving the unknown displacement increments, Δ_1 and Δ_2, are obtained by imposing continuity of average tractions increments across the (top and bottom) interfaces between the outer blocks and the cell.

The average equivalent strain in the band, $E^{\mathrm{b}}_{\mathrm{eq}}$, and that in the outer blocks, E_{eq}, play important roles in the results. The former is defined in as follows. Noting from (2.8) and (2.9) that the strain

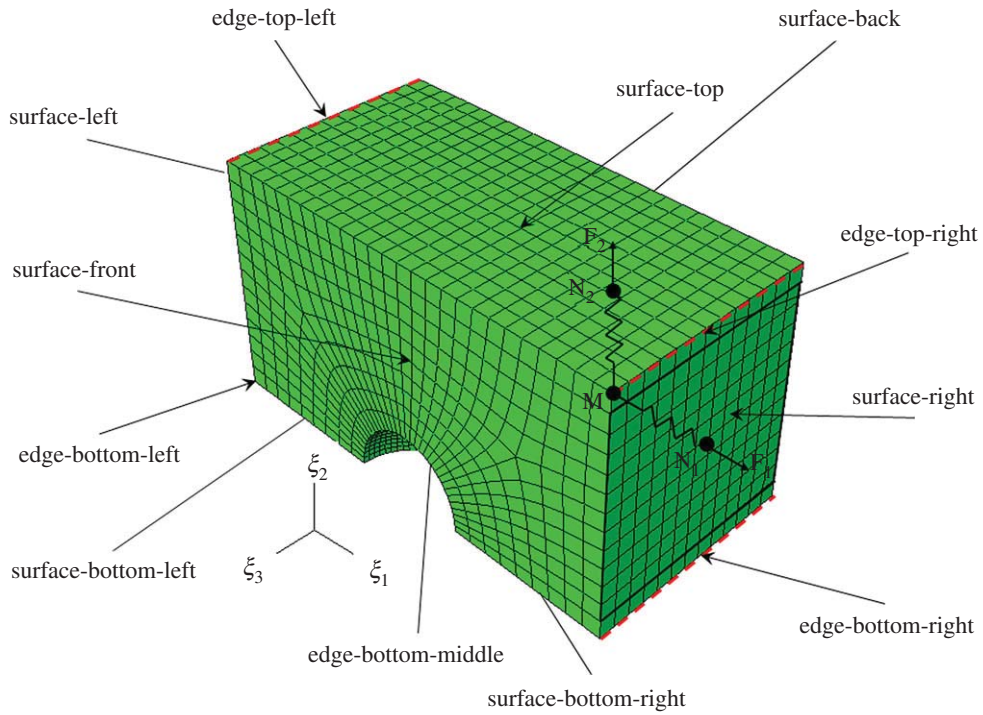

Figure 3. Finite-element mesh for the one-fourth of the unit cell used for modelling the band —see also figure 2—together with the nomenclature denoting different surfaces and edges to which the boundary conditions are applied. The origin of the reference coordinate system, ξ_i, corresponds to the centre of the void in the undeformed configuration. For the unit cell shown, the initial porosity is $f_0 = 0.01$, the initial orientation angle of the band is $\psi^u = 0^\circ$. Unlike for $\psi^u = 0^\circ$, for $\psi^u \neq 0^\circ$, the x_1 and ξ_1 are not coincident but separated by the angle ψ^u. For $\psi^u \neq 0^\circ$, the front and back faces of the unit cell take the form of a parallelogram as shown in figure 2 while the names of different surfaces and edges to which the boundary conditions are applied remain the same. The axes of the initially spherical void are aligned along the ξ_i coordinate axes for all values of ψ^u. (Online version in colour.)

in the band is the sum of the uniform strain outside the band plus the additional strain associated with the displacements, Δ_1 and Δ_2, one can express the average Eulerian strain rate in the band by

$$\left.\begin{aligned} D^b_{11} &= \cos^2(\psi)\dot{E}_{11} + \sin^2(\psi)\dot{E}_{22}, D^b_{33} = \dot{E}_{33}, \\ D^b_{22} &= \cos^2(\psi)\dot{E}_{22} + \sin^2(\psi)\dot{E}_{11} + \frac{2\dot{\Delta}_2\cos(\psi) - 2\dot{\Delta}_1\sin(\psi)}{H} \\ \text{and} \quad 2D^b_{12} &= \sin(2\psi)(\dot{E}_{22} - \dot{E}_{11}) + \frac{2\dot{\Delta}_1\cos(\psi) + 2\dot{\Delta}_2\sin(\psi)}{H} \end{aligned}\right\} \tag{2.11}$$

Here, the components of D^b_{ij} are expressed in the band coordinates ξ_i, whereas the components of the strain rate in the outer blocks, $\dot{E}_{ij}$, are with respect to x_i. The current thickness of the band is H, which evolves according to $\dot{H} = D^b_{22}H$. The equivalent strain rate in the band is the logarithmic rate, $\dot{E}^b_{eq} = \sqrt{3D^b_{ij}D^b_{ij}/2}$, with $E^b_{eq} = \int \dot{E}^b_{eq}$ as the accumulated value. The equivalent strain in the outer blocks, E_{eq}, is defined similarly with $\dot{E}_{eq} = \sqrt{3(\dot{E}^2_{11} + \dot{E}^2_{22} + \dot{E}^2_{33})/2}$.

Following the same approach as [34,49], let N_{ij} be the Cartesian components of the unsymmetrical nominal stress tensor (the first Piola–Kirchoff stress). Throughout the remainder of the paper, when a quantity is defined both for the outer blocks and the band, the quantity

corresponding to the band is distinguished by a superscript 'b'. Continuity of average normal and tangential traction rates across the band interfaces dictates

$$\dot{\bar{N}}_{22}^{\mathrm{b}\xi} = \frac{1}{A^{\mathrm{T}}}\int_A \dot{N}_{22}^{\mathrm{b}\xi}\ \mathrm{d}A^{\mathrm{T}} = \dot{N}_{22}^{\xi}, \quad \dot{\bar{N}}_{21}^{\mathrm{b}\xi} = \frac{1}{A^{\mathrm{T}}}\int_A \dot{N}_{21}^{\mathrm{b}\xi}\ \mathrm{d}A^{\mathrm{T}} = \dot{N}_{21}^{\xi}, \tag{2.12}$$

where $\dot{\bar{N}}_{ij}^{\mathrm{b}\xi}$ denote the average nominal traction rates on the top and bottom surfaces of the unit cell with respect to the ξ coordinate system (figure 1), and the integration is carried out over A^{T} the area of the top surface of the cell in the current configuration (the electronic supplementary material). The top and bottom surfaces of the band, as well as the ξ_i coordinate system attached to the band, rotate with the cell. In the FE simulations, it is convenient to work in the x_i coordinate system. Therefore, it is necessary to transform (2.12) to the x_i coordinates as now described.

The nominal stress rates in (2.12) and the Cartesian components of the Jaumann stress rate are related through

$$\dot{N}_{ij} = \hat{\dot{\Sigma}}_{ij} - \Sigma_{jk}\dot{E}_{ki} + \Sigma_{ik}W_{jk} + \Sigma_{ij}\dot{E}_{kk}, \tag{2.13}$$

with $W_{ij} = (\dot{u}_{i,j} - \dot{u}_{j,i})/2$ as the rotation rate. The outer blocks do not rotate with respect to the x_i axes, and thus (2.13) immediately provides the connection between the two stress rates in the blocks. By enforcing continuity of tractions across the (top and bottom) interfaces between the outer blocks and the cell, the force increments exerted by the blocks on the top surface of the unit cell read

$$\dot{F}_2 = A^{\mathrm{T}}\dot{N}_{22}\cos(\psi), \quad \dot{F}_1 = -A^{\mathrm{T}}\dot{N}_{11}\sin(\psi), \tag{2.14}$$

where ψ is the current orientation angle of the band and A^T is the current area of the top (or the bottom) surface of the cell. The force increments given in (2.14) are used to determine the corresponding displacement increments, $\dot{\Delta}_1$ and $\dot{\Delta}_2$, as detailed in the electronic supplementary material.

In this paper, attention is restricted to a square doubly periodic array of initially spherical voids of radius R_0 whose centres lie on the mid-plane of the band and whose centre-to-centre spacing in the initial state is $2L_0$ in both the ξ_1- and ξ_3-directions. The initial thickness of the band is taken to be $2L_0$ such that the initial volume of the unit cell is $V^{\mathrm{cell}} = 8L_0^3$ (figure 2). The initial void to cell volume fraction is used to characterize the void volume fraction in the band

$$f_0 = \frac{V^{\mathrm{void}}}{V^{\mathrm{cell}}} = \frac{\pi}{6}\left(\frac{R_0}{L_0}\right)^3, \tag{2.15}$$

with $\chi_0 = R_0/L_0$ as the radius to half-cell size ratio, it follows that $\chi_0 = (6f_0/\pi)^{1/3}$; these equations are valid for any initial orientation angle of the band, ψ^{u}.

The computational model is reduced to the analysis of a single unit cell with a set of boundary conditions derived from conditions of continuity of displacements and average tractions across the band/block interface and from periodicity conditions on the cell surfaces within the band. Prior to the onset of macroscopic localization, increments of Δ_1 and Δ_2 can be prescribed with the increments of the stresses and strains in the outer blocks as computed quantities. For a normal band ($\psi^{\mathrm{u}} = 0^\circ$), increments of Δ_2 can be prescribed and the normal traction computed (see the electronic supplementary material). Beyond the onset of macroscopic localization, one is required to prescribe some combination of increments of Δ_1 and Δ_2, because the outer blocks undergo elastic unloading with almost no further straining. The combination of increments of Δ_1 and Δ_2 that occurs beyond macroscopic localization is not unique in that it depends on the manner in which the motion of the outer blocks is constrained. In the simulations of coalescence following the onset of macroscopic localization in this paper, we have set the ratio of the increments, $\dot{\Delta}_1/\dot{\Delta}_2$, to be the same as that occurring just prior to the onset of macroscopic localization. This continues the straining in the band in an approximately proportional manner which should lead to coalescence with the least straining beyond the onset of macroscopic localization.

Owing to the symmetries involved in the problem, attention can be confined to a reduced cell one quarter of the unit cell, as shown in figure 3. The FE calculations are performed within a finite strain setting employing J_2 flow theory, using the commercial software Abaqus [50]. Results will be presented for cases in which the band is normal to the maximum principal stress ($\psi^{\mathrm{u}} = 0^\circ$) and cases in which the initial band angle is oriented to give the smallest value of E_{eq} at first localization, referred to in the sequel as the critical band orientation, ψ^{cu}. To obtain the critical orientation, simulations are repeated for many specific initial angles over a range of contending orientations. In this paper, the search for the critical initial band orientation resolves this angle to within about 3°. Further details related to the computations and to implementation of the boundary conditions are given in the electronic supplementary material.

3. The competition between macroscopic localization and void coalescence

As discussed in the Introduction, the aim of this study is to quantify the occurrence of two distinct types of localizations, designated here as macroscopic localization owing to void growth and localization owing to void coalescence. Results of numerical simulations using the band model described in §2 are presented which reveal when the two levels of localization occur simultaneously and when macroscopic localization precedes coalescence.

The computations have been carried out using the following inputs for the J_2 flow theory base material:

$$\sigma = \begin{cases} E\varepsilon & \text{if } \varepsilon \le \varepsilon_0, \\ \sigma_0 \left(\frac{\varepsilon}{\varepsilon_0}\right)^N & \text{if } \varepsilon > \varepsilon_0, \end{cases} \tag{3.1}$$

where σ_0 represents the initial yield stress, N is the strain-hardening exponent, E is the Young modulus and $\varepsilon_0 = \sigma_0/E$. The specific numerical values employed in generating the results are: $E = 167\,\mathrm{GPa}$ and $\sigma_0 = 418\,\mathrm{MPa}$, such that $\varepsilon_0 = 0.0025$, and $\nu = 0.3$. Of the inputs for the base material, the strain-hardening exponent has the most influence on the issues studied in this paper and results will be presented for $N = 0.1$ and 0.2.

(a) A specific case revealing the distinction between first localization and coalescence

To introduce the issues, detailed results are first presented for a specific case which has a clear separation between macroscopic localization induced by void growth softening and localization associated with void coalescence. Consider a material with a hardening exponent, $N = 0.1$, and an initial void volume fraction in the band, $f_0 = 0.001$. The overall macroscopic stress state in the blocks of material outside the band involves high triaxiality, $T = 3$, and an axisymmetric state with $\Sigma_{\mathrm{I}} > \Sigma_{\mathrm{II}} = \Sigma_{\mathrm{III}}$ ($L = -1$) is applied. Results will be presented for void growth and localization for a band oriented perpendicular to the maximum principal stress, $\psi^{\mathrm{u}} = 0^\circ$, as well as for the critical band orientation, $\psi^{\mathrm{u}} = \psi^{\mathrm{cu}}$.

The ratio of the effective strain in the band to the effective strain in the blocks outside the band is plotted against the effective strain in the blocks, E_{eq} in figure 4*a*, with a similar plot for the ratio of the void volume fraction to the initial void volume fraction in figure 4*b*. Macroscopic localization occurs when plastic straining ceases in the outer blocks with continuing plastic deformation in the band. The macroscopic localization is marked by the 'x' on these curves. Elastic unloading begins in the outer blocks at the point of first localization; however, this is not evident in the plots in figure 4, because the change in effective strain in the blocks is very small after the onset of localization. Effectively, the outer blocks appear rigid after the onset of localization. Coalescence localization sets in, as marked by the 'filled circles' on the curves, after much larger strains occur within the band and when the void volume fraction reaches about 10 times that at first localization. The definition of the onset of coalescence is given in the next paragraph. For the normal band, $\psi^{\mathrm{u}} = 0^\circ$, first localization begins at $E_{\mathrm{eq}} \cong 0.02$ when $E^{\mathrm{b}}_{\mathrm{eq}} \cong 0.03$ with $f/f_0 \cong 6$, whereas coalescence begins when $E^{\mathrm{b}}_{\mathrm{eq}} \cong 0.08$ and $f/f_0 \cong 80$. The corresponding values for the critical band angle are $E_{\mathrm{eq}} \cong 0.01$, $E^{\mathrm{b}}_{\mathrm{eq}} \cong 0.02$ and $f/f_0 \cong 3$ at first localization with $E^{\mathrm{b}}_{\mathrm{eq}} \cong 0.10$ and

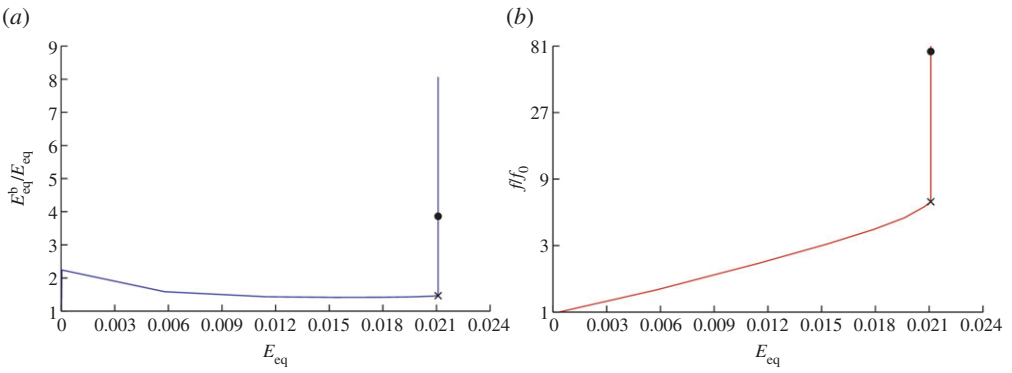

Figure 4. Evolution of (*a*) E^b_{eq}/E_{eq}, and (*b*) f/f_0 with E_{eq} for $f_0 = 0.001$, $T = 3.00$, $L = -1$, $N = 0.1$ and $\psi^u = 0^\circ$. The vertical axis is plotted by using a base 10 logarithmic scale for (*b*). (Online version in colour.)

$f/f_0 \cong 28$ at the onset of coalescence. These values regarding the strain and porosity at the onset of void coalescence agree with earlier results of 'classical' void cell calculations with fully periodic boundary conditions [48]. The critical band orientation is $\psi^u = 39^\circ$ in the undeformed state and $\psi^c \cong 39.5^\circ$ at the onset of first localization.

The distinction between the first (macroscopic) localization and coalescence localization is evident in figure 5 which reveals the distribution of effective plastic strain rate in the cell following the two localization events for both the normal band and the critical band orientation. Immediately after the first localization, the void continues to undergo nearly spherical expansion with significant continued straining above and below the void as well as in the ligaments between neighbouring voids in the band. Interaction between voids is occurring but the deformation is dominated by spherical expansion of the void. The softening necessary to give rise to the localization of deformation is due to the growth of the voids and is not a consequence of coalescence between voids. By contrast, after the onset of the coalescence localization, the effective strain rate in the cell is much larger in the ligaments than in the regions away from the plane of ligaments. Void growth is no longer even approximately spherical. Instead, the equator of the void expands laterally within the band, whereas the patches of area of the void surface farthest from the void plane undergo little additional straining. After the onset of the coalescence localization almost all the additional plastic deformation is confined to the ligaments between the voids, as envisioned in the early modelling of coalescence of Thomason [36] and subsequent researchers [28,31]. In this paper, the definition of the onset of coalescence is taken to be that point in the history when the ratio of the maximum to the minimum effective plastic strain rate at the void surface first exceeds 15. Alternative choices for this ratio, for example using 10 or 20, would make relatively little difference in the results presented for the onset of coalescence in this paper. In the example in figure 4, even though the void has expanded in volume by a factor of about 10 from first localization to the onset of coalescence, its volume fraction is still relatively small when coalescence begins, i.e. $f \cong 0.07$.

Figure 6 shows the average true stress and nominal stress perpendicular to the band plotted against the average effective strain in the band for the case when the band is oriented perpendicular to the maximum principal stress ($\psi^u = 0^\circ$). At this level of high triaxiality, there is little difference in the two stress quantities, because the overall deformation remains relatively small. After localization starts, the changes in the true stress and the nominal stress are essentially identical, because elastic unloading in the outer blocks effectively suppresses any significant area change of the block/band interface. The two stress quantities decrease with increasing strain in the band until coalescence localization begins, as marked by the 'filled circles'. In this example, the stress at the onset of coalescence is considerably below the stress at first localization. While first localization produces a sharp change in the slope of the curve of stress versus strain in the

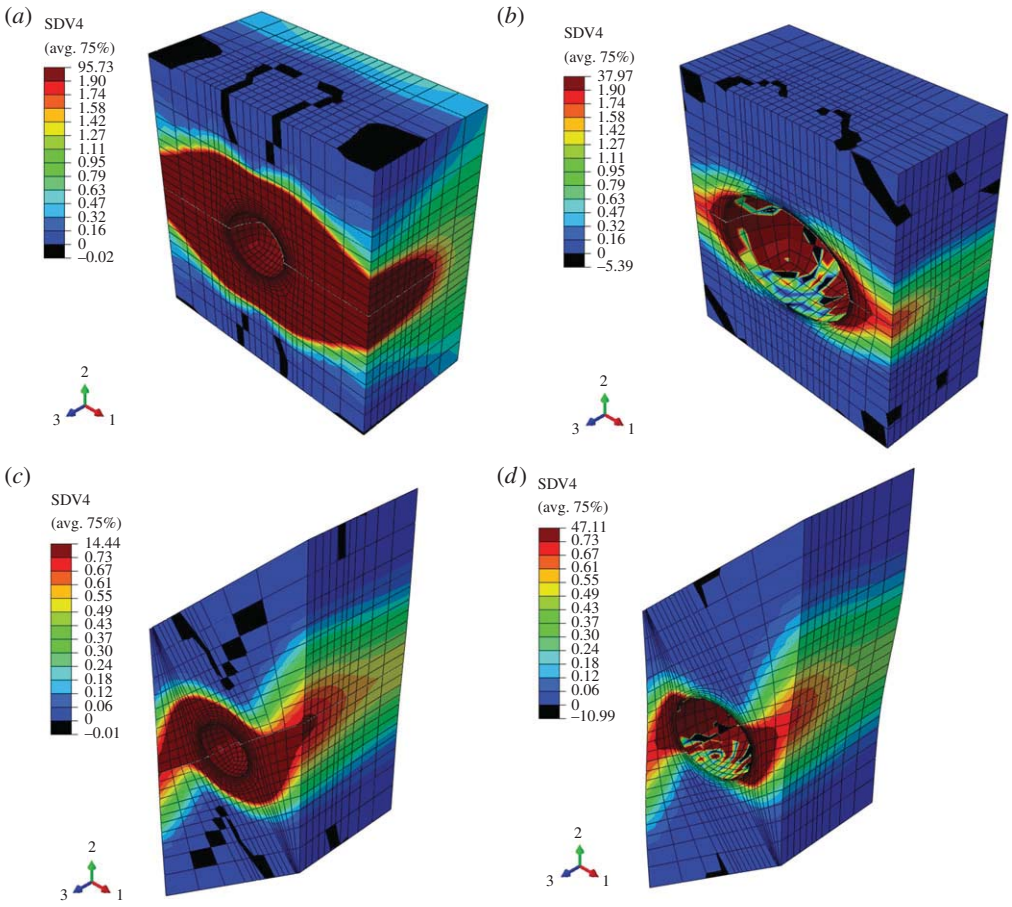

Figure 5. Distribution of the equivalent strain rate: (*a*,*c*) at the onset of the macroscopic localization of the plastic flow in the band, and (*b*,*d*) at the onset of void coalescence. For all four figures, $f_0 = 0.001$, $T = 3.00$, $L = -1$ and $N = 0.1$. $\psi^{\mathrm{u}} = 0^\circ$ for (*a*) and (*b*), and $\psi^{\mathrm{u}} = 39^\circ$ for (*c*,*d*). All meshes are plotted in the deformed configuration. (Online version in colour.)

band in figure 6, the subsequent onset of coalescence is not accompanied by a notable slope change. For $\psi^{\mathrm{u}} = 0^\circ$, beyond the onset of the first localization, the outer blocks constrain the deformation in the cell to be uniaxial straining on average. Owing to this constraint, the stress triaxiality within the band generally increases sharply following localization, thereby promoting further void growth and the onset of coalescence. This feature was captured in an early model of void growth within a normal localization band by Andersson [51]. Models with periodicity conditions imposed on all faces of the representative void-containing cell generally take the stress triaxiality within the cell to be constant throughout the entire deformation history and therefore do not reflect the influence of enhanced triaxiality that accompanies localization.

(b) The effect of stress triaxiality on localization and coalescence for axisymmetric stress states ($L = -1$)

Figure 7 shows the effective strain in the band at the onset of first localization and at the onset of coalescence as a function of the prescribed stress triaxiality in the outer blocks, T, for two values of the initial void volume fraction, $f_0 = 0.001$ and $f_0 = 0.01$ and for two values of the strain-hardening exponent, $N = 0.1$ and 0.2. The band angle, $\psi^{\mathrm{u}} = 0^\circ$, has been restricted to be perpendicular to the maximum principal stress in these simulations. It is essential to plot the strain in the band, $E^{\mathrm{b}}_{\mathrm{eq}}$,

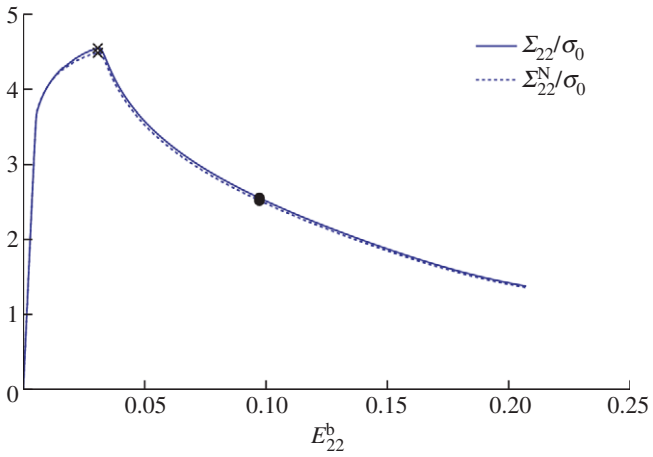

Figure 6. Variation of normalized true stress Σ_{22}/σ_0 and normalized nominal stress Σ^{N}_{22}/σ_0 with E^{b}_{22} for $f_0 = 0.001$, $T = 3.00$, $L = -1$, $N = 0.1$ and $\psi^{u} = 0^{\circ}$. The cross indicates the onset of the macroscopic localization of the plastic flow in the band, whereas the solid dot indicates the onset of void coalescence. (Online version in colour.)

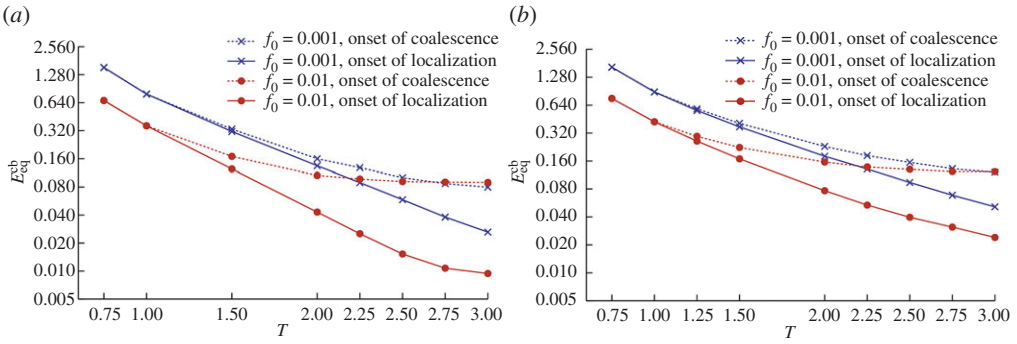

Figure 7. Values of E^{cb}_{eq} at first localization and at the onset of coalescence as a function of T for $L = -1$, $\psi^{u} = 0^{\circ}$; $N = 0.1$ for (*a*), and $N = 0.2$ for (*b*). The vertical axis is plotted by using a base 10 logarithmic scale for both figures. (Online version in colour.)

rather than the strain outside the band E_{eq} to reveal the separation between first localization and coalescence because, as noted above, the strain outside the band undergoes very little change in strain after the onset of the first localization. It is significant that for each case considered in figure 7, a clear separation between macroscopic localization and coalescence localization occurs for $T > 1$, whereas for $T < 1$, the onset of first localization is essentially simultaneous with coalescence. The transition value, $T \cong 1$, has been found in all the simulations with the present model, for both the normal band orientation and for the critical orientation. *Thus, for* $L = -1$, *the present model predicts that the onset of localization is coincident with void coalescence at stress triaxialities below* $T \cong 1$ *and that void coalescence occurs subsequent to macroscopic localization for* $T > 1$. We return to this transition in the final discussion in the paper where the issue of whether the perfect void alignment assumed in the present model may unrealistically favour the onset of coalescence.

In addition to the strong dependency on triaxiality, figure 7 reveals that the first (macroscopic) localization has a strong dependence on both the initial void volume fraction, f_0, and the strain-hardening index, N, as expected. In the range of high triaxiality, the onset coalescence localization is less sensitive to these parameters. Companion results for the history of the true and nominal stress normal to the band are plotted in figure 8. The growth history of the void is plotted as f/f_0

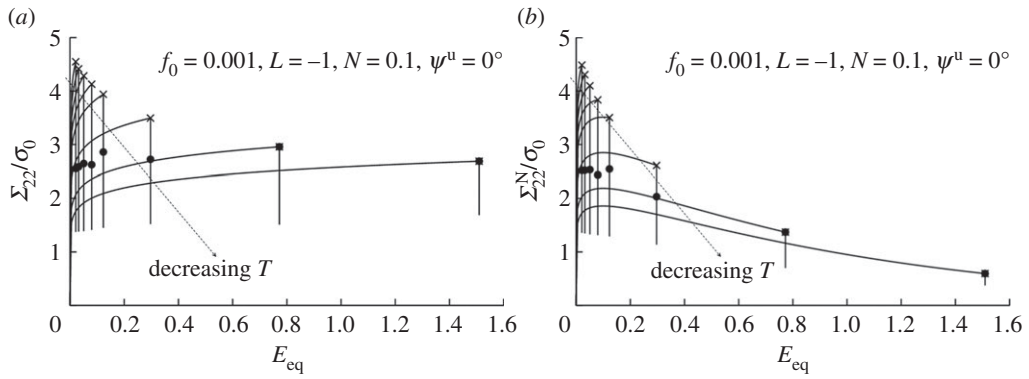

Figure 8. Variation of (*a*) normalized true stress Σ_{22}/σ_0 and (*b*) normalized nominal stress Σ^N_{22}/σ_0 with E_{eq}. Both (*a*) and (*b*) show seven different curves, each corresponding to one of $T = 0.75, 1.00, 1.50, 2.00, 2.25, 2.50, 2.75, 3.00$. The cross indicates the onset of macroscopic localization, whereas the solid dot indicates the onset of void coalescence.

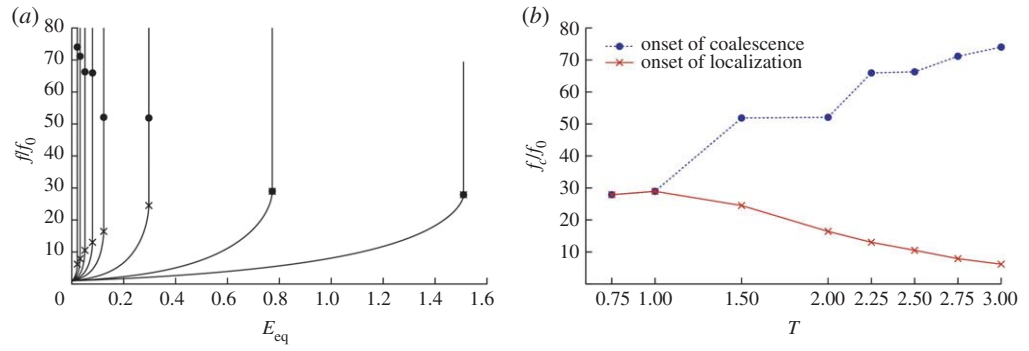

Figure 9. Variation of (*a*) f/f_0 with E_{eq} and (*b*) f_c/f_0 with T for $f_0 = 0.001, L = -1, N = 0.1$ and $\psi^u = 0°$. The cross indicates the onset of the macroscopic localization, whereas the solid dot indicates the onset of void coalescence. (Online version in colour.)

versus E_{eq} in figure 9*a* and the values of f/f_0 at first localization and at the onset of coalescence as a function of T in figure 9*b*. The separation between first localization and coalescence for $T > 1$ is brought out clearly in the latter figure. Figure 9*b* also reveals that there is some uncertainty in identifying the onset of coalescence owing to the fact that each simulation must be monitored step by step to identify the point where the localization condition is met. For $T < 1$, the onset of localization and coalescence occurs when the void volume fraction reaches $f \cong 0.03$ in this example, a relatively small value which, nevertheless, is 30 times the initial value. Thus, while macroscopic localization and coalescence occur simultaneously when $T < 1$, extensive prior void growth has occurred to set the stage for these events which is not predicted by a coalescence model. This illustrates the important point that, even though macroscopic localization and coalescence occur simultaneously, a coalescence analysis by itself cannot be used to predict the dependence of localization on the initial void volume fraction.

The results for the effective strain in the band at first localization and at the onset of coalescence as a function of T are plotted in figure 10 for the critical band angle where they can be compared with the corresponding results for the case with the normal band, $\psi = 0°$. In addition, the macroscopic effective strain in the outer blocks, E_{eq}, at first localization is plotted in figure 11. As emphasized earlier, the value of E_{eq} at first localization is a measure of macroscopic ductility. The critical band orientations in the undeformed state and at first localization are plotted in figure 12. It is interesting to note that the value of the critical angle does not change significantly

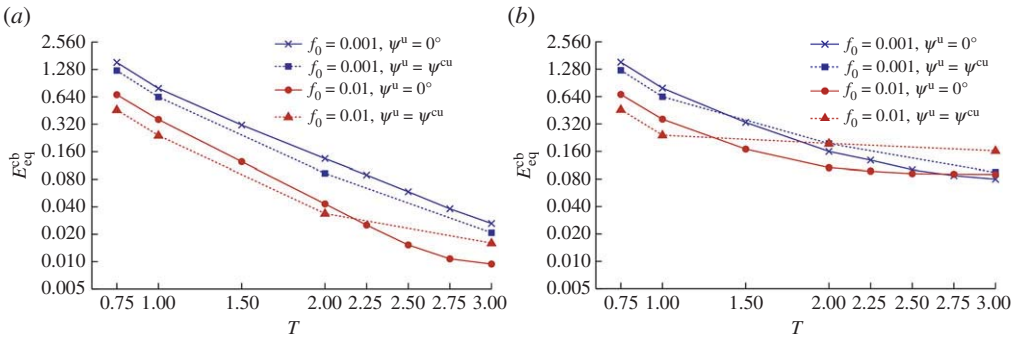

Figure 10. Values of the critical effective strain in the band, E^{cb}_{eq}, at the onset of first localization in (*a*) and at the onset of coalescence in (*b*) as a function of T for $L = -1$ and $N = 0.1$. The dashed lines are associated with the critical band orientation, whereas the solid lines correspond to the band orientation normal to the maximum principal stress. The vertical axis is plotted by using a base 10 logarithmic scale for both figures. The seemingly anomalous points at the highest levels of T for $f = 0.01$ are related to the fact that outer blocks do not begin to yield plastically. The effective strain in the outer blocks in these cases is less for the critical band orientation than for the normal band. (Online version in colour.)

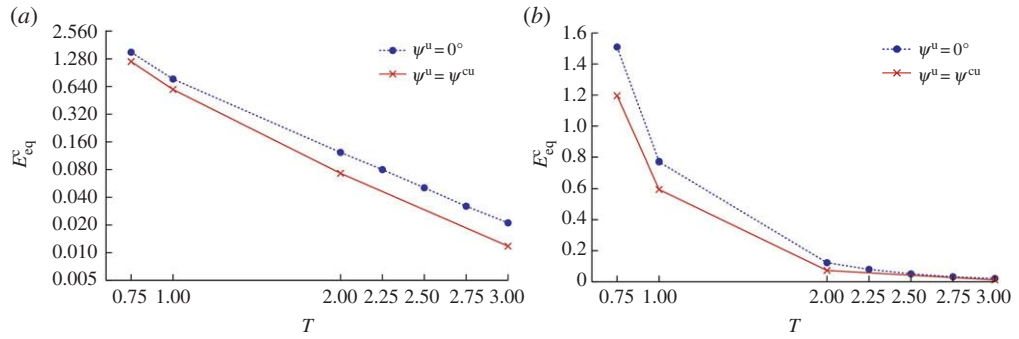

Figure 11. Variation the critical equivalent strain outside the band at first localization, E^{c}_{eq}, as a function of T for $f_0 = 0.001$, $L = -1$ and $N = 0.1$. The critical strain for the normal band orientation and for the critical band orientation are shown. The vertical axis uses a base 10 logarithmic scale for (*a*). (Online version in colour.)

for triaxialities above or below the transition at $T \cong 1$. Furthermore, the difference between the localization strain as a function of the band angle remains moderate.

(c) The effect of the lode parameter on the two localizations

The role of the Lode parameter on void growth and macroscopic localization has been studied extensively in references [15,16,47]. These studies have shown that, at a given triaxiality T, the smallest effective strain at first localization is associated with shearing stress states ($L = 0$), see also [17]. Here, the primary objective is to reveal the role that the Lode parameter plays in the competition between first localization and coalescence. For $N = 0.1$ and $f_0 = 0.001$, figure 13 plots the effective strain in the band, E^{b}_{eq}, at first localization and at the onset of coalescence as a function of T for shearing stress states ($L = 0$) and for both types of axisymmetric stress states, $\Sigma_I > \Sigma_{II} = \Sigma_{III}$ ($L = -1$) and $\Sigma_I = \Sigma_{II} > \Sigma_{III}$ ($L = 1$). The macroscopic effective strain at first localization, E^{c}_{eq}, is shown in figure 14. The results in figures 13 and 14 are associated with the critical band orientation. Figure 13 indicates that the separation trend between first localization and the onset of coalescence is similar over the entire range of the Lode parameter with first localization and coalescence being coincident for $T < 1$. Thus, it appears that the Lode angle does not play a strong role in determining the value of triaxiality at the transition from macroscopic

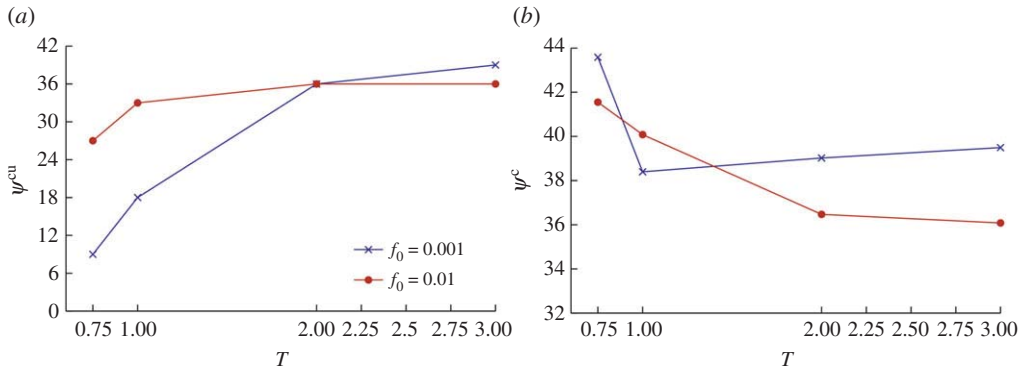

Figure 12. Variation with respect to T of the critical band orientation in the undeformed state, ψ^{cu}, in (*a*) and in the deformed state, ψ^{c}, in (*b*) for $L = -1$ and $N = 0.1$. (Online version in colour.)

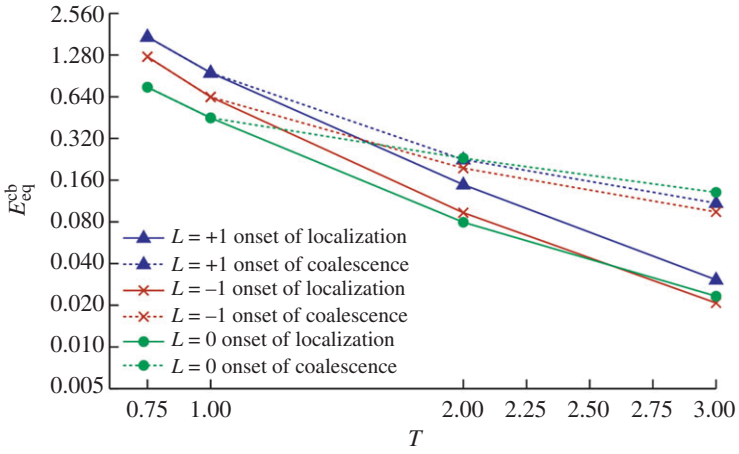

Figure 13. The dependence of the variation of the critical effective strains in the band, E^{cb}_{eq}, with T on the Lode parameter, L, for $f_0 = 0.001$, $N = 0.1$, at the critical band orientation. The vertical axis is plotted by using a base 10 logarithmic scale. (Online version in colour.)

localization to coalescence. In addition, the trend of relative magnitudes of the localization strains for the three types of stress states, $L = -1$, 0, 1, with T in figure 14 is similar to that found in references [15,16].

It is worth noting that the slope of the dependence of $\log E_{eq}$ versus T in figure 14*a* is essentially the same for the three values of the Lode parameter: $\mathrm{d}(\log E_{eq})/\mathrm{d}T = 3q_1/2$, where $q_1 \cong 1.3$. This value is not very different from values of the similarly defined factor q_1 Tvergaard introduced to calibrate the Gurson model, see [5].

4. Discussion and conclusion

Compared with a majority of earlier analyses of void growth and coalescence based on FE cell calculations with fully periodic conditions, the FE framework developed for this study allows macroscopic localization to be explicitly simulated owing to the embedding of an internal porous layer inside two semi-infinite non-porous outer blocks. Earlier axisymmetric analyses which approximate periodic conditions have shown that the onset of coalescence sometimes occurs after the maximum true stress peak is attained, indicating that macroscopic localization can take place

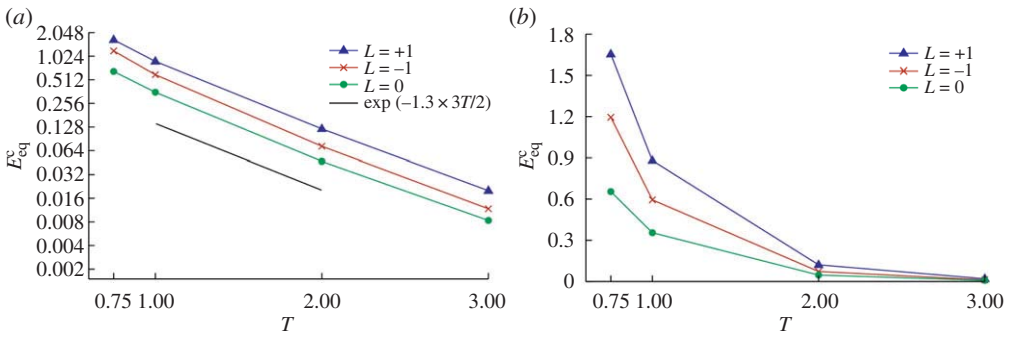

Figure 14. Variation of the equivalent strain in the outer blocks at first localization, E^c_{eq}, with T for three values of the Lode parameter, L, for $f_0 = 0.001$, $N = 0.1$, and at the critical band orientation. The vertical axis is plotted by using a base 10 logarithmic scale for (*a*). It is worth noting that the slope of the dependence of log E_{eq} versus T in (*a*) is essentially the same for each of the three computed curves: $\mathrm{d}(\log E_{eq})/\mathrm{d}T = 3q_1/2$, where $q_1 \cong 1.3$. (Online version in colour.)

prior to void coalescence. In these calculations, constant stress triaxiality is enforced in the porous cell throughout the simulation. However, the present framework captures the change of constraint occurring in the band after macroscopic localization when the stress triaxiality may increase dramatically, hence accelerating the occurrence of the void coalescence mechanism. Furthermore, the present framework accounts for all possible band orientations identifying the orientation corresponding to the earliest possible macroscopic localization. The main results that emerge from the present investigation are the following:

— The transition between macroscopic localization preceding coalescence and the simultaneous occurrence of macroscopic localization occurs at a stress triaxiality around 1. In the simulations carried out here, this transition is relatively independent of the initial void volume fraction, the strain-hardening exponent and the Lode parameter. At a triaxiality larger than 1, a macroscopic localization band occurs with void coalescence requiring additional plastic straining in the band. One implication is that at high stress triaxiality, the proper failure criterion to be used for engineering fracture analysis should be a macroscopic localization criterion based on void growth and not one based on void coalescence. The difference between such predictions can be significant when the triaxiality is high.

— This conclusion does not mean that a void coalescence criterion is not needed for high stress triaxiality fracture modelling. For example, in simulations of ductile crack propagation in a solid described by a porous plasticity model, such as the Gurson model or other such models, macroscopic localization will emerge naturally, but void coalescence must be properly modelled to accurately account for all the energy dissipated in the failure process.

— When macroscopic localization dominates, the effect of the strain-hardening exponent is, as expected, a key parameter in establishing the strain to localization. The material more effectively resists fracture when the strain-hardening capacity is high. A high strain-hardening capacity, all other parameters taken constant, thus promotes higher fracture toughness.

— As predicted in earlier studies, the critical band orientation leading to the smallest localization strain is not normal to the maximum principal stress but instead closer to 45° in the deformed configuration, independent whether macro localization precedes the coalescence or is simultaneous with it. Nevertheless, the difference between the strains at localization obtained for different angles is not very large. This means that in a structural alloy, the band orientation might be dictated, for example, by the direction in which the

voids are aligned most closely in the processing history. It is also notable that, in line with recent work, this study shows that the lowest localization strains at a given triaxiality occur when the Lode parameter is zero, corresponding to shearing stress states.

The model used in this study, and, indeed, those used in nearly all previous computational models of void growth and interaction, consider periodic arrays of aligned voids. The reason for this is obvious—it allows for much smaller computations employing a unit cell containing a single void with periodic boundary conditions. Intuitively, it seems reasonable to suspect that highly aligned void ligaments would lead to early coalescence, compared with more random void arrangements. If this is the case, then the transition between simultaneous and separated macroscopic localization and coalescence predicted by the present model at $T \cong 1$ is too high. It will be important to address this question in the future as well as the effect of multiple rows of voids in the unit cell. As noted in connection with *mechanism 5* in figure 1, the role of clusters of voids on initiation of localization, microcracking and ductile tearing has received relatively little attention, even though observations in a variety of industrial metallic alloys suggest such behaviour is important. The role of triaxiality on critical cluster size [52] and the issue of localization owing to void growth as opposed to void coalescence are largely unexamined at the present time (see also the recent study [53]).

Acknowledgements. The support of the Belgian Science Policy through the IAP 7/21 project is gratefully acknowledged.

References

1. Rogers HC. 1960 The tensile fracture of ductile metals. *Trans. Met. Soc. AIME* **218**, 498–506.
2. McClintock FA. 1968 A criterion for ductile fracture by the growth of voids. *J. Appl. Mech.* **35**, 363–371. (doi:10.1115/1.3601204)
3. Rice JR, Tracey DM. 1969 On the ductile enlargement of voids in triaxial stress fields. *J. Mech. Phys. Solids* **17**, 201–217. (doi:10.1016/0022-5096(69)90033-7)
4. Pineau A. 1981 Review of fracture micromechanisms and a local approach to predicting crack resistance in low strength steels. In *Advances in fracture research, ICF5* (ed. D François), pp. 553–577. Oxford, UK: Pergamon Press.
5. Tvergaard V. 1990 Material failure by void growth to coalescence. *Adv. Appl. Mech.* **27**, 83–151. (doi:10.1016/S0065-2156(08)70195-9)
6. Pineau A, Pardoen T. 2007 Failure mechanisms of metals. In *Comprehensive structural integrity encyclopedia* (eds B Karihaloo and WG Knauss), vol. 2, ch. 6. Amsterdam, The Netherlands: Elsevier.
7. Needleman A, Tvergaard V. 1987 An analysis of ductile rupture modes at a crack tip. *J. Mech. Phys. Solids* **35**, 151–183. (doi:10.1016/0022-5096(87)90034-2)
8. Xia L, Shih CF, Hutchinson JW. 1995 A computational approach to ductile crack growth under large scale yielding conditions. *J. Mech. Phys. Solids* **43**, 389–413. (doi:10.1016/0022-5096(94)00069-H)
9. Brocks W, Klingbeil D, Künecke G, Sun D-Z. 1995 Application of the Gurson model to ductile tearing resistance. In *Constraint effects in fracture theory and++ applications, ASTM STP 1244* vol. 2 (eds M Kirk, A Bakker), pp. 232–252. Philadelphia, PA: The American Society for Testing and Materials.
10. Koppenhoefer KC, Dodds Jr RH. 1998 Ductile crack growth in pre-cracked CVN specimens: numerical studies. *Nucl. Eng. Des.* **180**, 221–241. (doi:10.1016/S0029-5493(97)00218-5)
11. Pardoen T, Scheyvaerts F, Simar A, Tekoğlu C, Onck PR. 2010 Multiscale modeling of ductile failure in metallic alloys. *C. R. Phys.* **11**, 326–345. (doi:10.1016/j.crhy.2010.07.012)
12. Brunet M, Morestin F, Walter H. 2004 Damage identification for anisotropic sheet-metals using a non-local damage model. *Int. J. Damage Mech.* **13**, 35–57. (doi:10.1177/1056789504039259)
13. Lassance D, Fabrègue D, Delannay F, Pardoen F. 2007 Micromechanics of room and high temperature fracture in 6xxx Al alloys. *Prog. Mater. Sci.* **52**, 62–129. (doi:10.1016/j.pmatsci.2006.06.001)

14. Chéhab B, Bréchet Y, Véron M, Jacques PJ, Parry G, Mithieux J-D, Glez J-C, Pardoen T. 2010 Micromechanics of the high temperature damage in a dual phase stainless steel. *Acta Mater.* **58**, 626–637. (doi:10.1016/j.actamat.2009.09.041)
15. Barsoum I, Faleskog J. 2011 Micromechanical analysis on the influence of the Lode parameter on void growth and coalescence. *Int. J. Solids Struct.* **48**, 925–938. (doi:10.1016/j.ijsolstr.2010.11.028)
16. Dunand M, Mohr D. 2014 Effect of Lode parameter on plastic flow localization after proportional loading at low stress triaxialities. *J. Mech. Phys. Solids* **66**, 133–153. (doi:10.1016/j.jmps.2014.01.008)
17. Scheyvaerts F, Onck PR, Tekoğlu C, Pardoen T. 2011 The growth and coalescence of ellipsoidal voids in plane strain under combined shear and tension. *J. Mech. Phys. Solids* **59**, 373–397. (doi:10.1016/j.jmps.2010.10.003)
18. Bao Y, Wierzbicki T. 2004 On fracture locus in the equivalent strain and stress triaxiality space. *Int. J. Mech. Sci.* **46**, 81–98. (doi:10.1016/j.ijmecsci.2004.02.006)
19. Rivalin F, Besson J, Pineau A, Di Fant M. 2001 Ductile tearing of pipeline-steel wide plates: II. Modeling of in-plane crack propagation. *Eng. Fract. Mech.* **68**, 347–364. (doi:10.1016/S0013-7944(00)00108-9)
20. Besson J, Steglich D, Brocks W. 2003 Modeling of plane strain ductile rupture. *Int. J. Plast.* **19**, 1517–1541. (doi:10.1016/S0749-6419(02)00022-0)
21. Pardoen T, Hutchinson JW. 2003 Micromechanics-based model for trends in toughness of ductile metals. *Acta Mater.* **51**, 133–148. (doi:10.1016/S1359-6454(02)00386-5)
22. Gullerud AS, Gao X, Dodds Jr RH, Haj-Ali R. 2000 Simulation of ductile crack growth using computational cells: numerical aspects. *Eng. Fract. Mech.* **66**, 65–92. (doi:10.1016/S0013-7944(99)00147-2)
23. Sobotka JC, Dodds Jr RH. 2011 Steady crack growth in a thin, ductile plate under small-scale yielding conditions: three-dimensional modeling. *Eng. Fract. Mech.* **78**, 343–363. (doi:10.1016/j.engfracmech.20.10.10.006)
24. Roychowdhury S, Roy YDA, Dodds Jr RH. 2002 Ductile tearing in thin aluminum panels: experiments and analyses using large-displacement, 3-D surface cohesive elements. *Eng. Fract. Mech.* **69**, 983–1002. (doi:10.1016/S0013-7944(01)00113-8)
25. Pardoen T, Hachez F, Marchioni B, Blyth PH, Atkins AG. 2004 Mode I fracture of sheet metal. *J. Mech. Phys. Solids* **52**, 423–452. (doi:10.1016/S0022-5096(03)00087-5)
26. Nielsen KL, Hutchinson JW. 2012 Cohesive traction–separation laws for tearing of ductile metal plates. *Int. J. Impact Eng.* **48**, 15–23. (doi:10.1016/j.ijimpeng.2011.02.009)
27. Lecarme L, Tekoğlu C, Pardoen T. 2011 Void growth and coalescence in ductile solids with stage III and stage IV strain hardening. *Int. J. Plast.* **27**, 1203–1223. (doi:10.1016/j.ijplas.2011.01.004)
28. Tekoğlu C, Leblond J-B, Pardoen T. 2012 A criterion for the onset of void coalescence under combined tension and shear. *J. Mech. Phys. Solids* **60**, 1363–1381. (doi:10.1016/j.jmps.2012.02.006)
29. Gologanu M, Leblond J-B, Perrin G, Devaux J. 1997 Recent extensions of Gurson's model for porous ductile metals. In *Continuum micromechanics, CISM lectures series* (ed P Suquet), pp. 61–130. New York, NY: Springer.
30. Benzerga AA, Besson J, Pineau A. 2004 Anisotropic ductile fracture. Part II: theory. *Acta Mater.* **52**, 4639–4650. (doi:10.1016/j.actamat.2004.06.019)
31. Benzerga AA, Leblond J-B. 2010 Ductile fracture by void growth to coalescence. *Adv. Appl. Mech.* **27**, 83–151.
32. Keralavarma SM, Benzerga AA. 2008 An approximate yield criterion for anisotropic porous media. *C. R. Méch.* **336**, 685–692. (doi:10.1016/j.crme.2008.07.008)
33. Morgeneyer TF, Helfen L, Mubarak H, Hild F. 2013 3D digital volume correlation of synchrotron radiation laminography images of ductile crack initiation: an initial feasibility study. *Exp. Mech.* **53**, 543–556. (doi:10.1007/s11340-012-9660-y)
34. Rice JR. 1976 The localization of plastic deformation. In *Theoretical and applied mechanics*, vol. 1 (ed. WT Koiter), pp. 207–220. Delft, The Netherlands: North-Holland Publishing.
35. Gurson A. 1977 Continuum theory of ductile rupture by void nucleation and growth: part I – yield criteria and flow rules for porous ductile media. *J. Eng. Mater. Technol.* **99**, 2–15. (doi:10.1115/1.3443401)
36. Thomason PF. 1990 *Ductile fracture of metals*. Oxford, UK: Pergamon Press.

37. Weck A, Wilkinson DS, Maire E. 2008 Observation of void nucleation, growth and coalescence in a model metal matrix composite using X-ray tomography. *Mater. Sci. Eng. A* **488**, 435–445. (doi:10.1016/j.msea.2007.11.050)
38. Lecarme L, Maire E, Kumar KCA, De Vleeschouwer C, Jacques L, Simar A, Pardoen T. 2014 Heterogenous void growth revealed by in situ 3-D X-ray microtomography using automatic cavity tracking. *Acta Mater.* **63**, 130–139. (doi:10.1016/j.actamat.2013.10.014)
39. Srivastava A, Ponson L, Osovski S, Bouchaud E, Tvergaard V, Needleman A. 2013 Effect of inclusion density on ductile fracture toughness and roughness. *J. Mech. Phys. Solids* **63**, 62–79. (doi:10.1016/j.jmps.2013.10.003)
40. Rice JR, Johnson MA. 1970 The role of large crack tip geometry changes in plane strain fracture. In *Inelastic behavior of solids* (eds MF Kanninen *et al.*), pp. 641–671. New York, NY: McGraw-Hill.
41. Tvergaard V, Hutchinson JW. 1992 The relation between crack growth resistance and fracture process parameters in elastic-plastic solids. *J. Mech. Phys. Solids* **40**, 1377–1397. (doi:10.1016/0022-5096(92)90020-3)
42. Worswick MJ, Chen ZT, Pilkey AK, Lloyd D, Court S. 2001 Damage characterization and damage percolation modeling in aluminum alloy sheet. *Acta Mater.* **49**, 2791–2803. (doi:10.1016/S1359-6454(01)00163-X)
43. Koplik J, Needleman A. 1988 Void growth and coalescence in porous plastic solids. *Int. J. Solids Struct.* **24**, 835–853. (doi:10.1016/0020-7683(88)90051-0)
44. Tvergaard V. 1982 On localization in ductile materials containing spherical voids. *Int. J. Fract.* **18**, 237–252. (doi:10.1007/BF00015686)
45. Tvergaard V. 1989 Numerical study of localization in a void-sheet. *Int. J. Solids Struct.* **25**, 1143–1156. (doi:10.1016/0020-7683(89)90073-5)
46. Marciniak Z, Kuczynski K. 1967 Limit strains in the processes of stretch-forming sheet metal. *Int. J. Mech. Sci.* **9**, 609–620. (doi:10.1016/0020-7403(67)90066-5)
47. Gao X, Kim J. 2006 Modeling of ductile fracture: significance of void coalescence. *Int. J. Solids Struct.* **43**, 6277–6293. (doi:10.1016/j.ijsolstr.2005.08.008)
48. Pardoen T, Hutchinson JW. 2000 An extended model for void growth and coalescence. *J. Mech. Phys. Solids* **48**, 2467–2512. (doi:10.1016/S0022-5096(00)00019-3)
49. Mear M, Hutchinson JW. 1985 Influence of yield surface curvature on flow localization in dilatant plasticity. *Mech. Mater.* **4**, 395–407. (doi:10.1016/0167-6636(85)90035-3)
50. ABAQUS. 2012 *The Abaqus documentation collection, Version 6.12*. Providence, RI: Dassault Systèmes.
51. Andersson H. 1977 Analysis of a model for void growth and coalescence ahead of a moving crack tip. *J. Mech. Phys. Solids* **25**, 217–233. (doi:10.1016/0022-5096(77)90024-2)
52. Ohno N, Hutchinson JW. 1984 Plastic flow localization due to non-uniform void distribution. *J. Mech. Phys. Solids* **32**, 63–85. (doi:10.1016/0022-5096(84)90005-X)
53. Roux E, Bernacki M, Bouchard PO. 2013 A level-set and anisotropic adaptive remeshing strategy for the modeling of void growth under large plastic strain. *Comp. Mater. Sci.* **68**, 32–46. (doi:10.1016/j.commatsci.2012.10.004)